Journal of Quantitative Spectroscopy & Radiative Transfer 195 (2017) 132–140

Contents lists available at ScienceDirect

Journal of Quantitative Spectroscopy & Radiative Transfer

journal homepage: www.elsevier.com/locate/jqsrt

Light scattering by ice crystals of cirrus clouds: From exact numerical methods to physical-optics approximation

Alexander Konoshonkin [a,b,*], Anatoli Borovoi [a], Natalia Kustova [a], Hajime Okamoto [c], Hiroshi Ishimoto [d], Yevgen Grynko [e], Jens Förstner [e]

[a] V. E. Zuev Institute of Atmospheric Optics SB RAS, Academician Zuev Sq. 1, 634055 Tomsk, Russia
[b] Tomsk State University, 36 Lenin Ave, 634050 Tomsk, Russia
[c] Kyushu University, Research Institute for Applied Mechanics, 6-1 Kasuga-koen Kasuga-city, Fukuoka 816-8580, Japan
[d] Meteorological Research Institute, Nagamine 1-1, Tsukuba 305-0052, Japan
[e] Department of Electrical Engineering, University Paderborn, Warburger Str. 100, 33098 Paderborn, Germany

ARTICLE INFO

Article history:
Received 14 September 2016
Received in revised form
8 December 2016
Accepted 8 December 2016
Available online 22 December 2016

Keywords:
Atmospheric scattering
Diffraction
Ice crystal phenomena
lidar

ABSTRACT

The problem of light scattering by ice crystals of cirrus clouds is considered in the case of a hexagonal ice plate with different distributions over crystal orientations. The physical-optics approximation based on (E, M)-diffraction theory is compared with two exact numerical methods: the finite difference time domain (FDTD) and the discontinuous Galerkin time domain (DGTD) in order to estimate its accuracy and limits of applicability. It is shown that the accuracy of the physical-optics approximation is estimated as 95% for the averaged backscattering Mueller matrix for particles with size parameter more than 120. Furthermore, the simple expression that allows one to estimate the minimal number of particle orientations required for appropriate spatial averaging has been derived.

1. Introduction

Light scattering by ice crystals of cirrus clouds is a challenging problem in the atmospheric optics. On the one hand, the radiative properties of cirrus clouds like the optical depth, extinction and scattering coefficients along with their phase function or, more generally, the Mueller matrix, are needed to incorporate in the numerical models of the Earth's radiative balance [1,2]. At present, these radiative properties are poorly known and they are one of the main sources of uncertainties in numerical climate models [3,4]. On the other hand, interpretation of the data obtained by remote sensing instruments sounding cirrus clouds should be based on the solution of the basic problem of light scattering by one ice crystal averaged over statistical ensembles of the crystals. This problem has not been satisfactorily solved yet [5]. The main obstacle in solving this problem is a great variation of the crystal size, where the size occurring in the cirrus range from a few microns up to millimeters [6,7].

Any numerical solution to the problem of light scattering by nonspherical particles crucially depends on the magnitude of the so-called size parameter. In this paper we define the size parameter as $s = 2\pi a/\lambda$, where a is the maximum size of the particle and λ is the incident wavelength, while previously we did not use the factor 2π. When the size parameter of the ice crystals is moderately small, e.g. $s \le 150$, a number of exact numerical methods based on the Maxwell equations such as the finite-difference time domain (FDTD) method [8–12], the T-matrix method [13–15], the discrete dipole approximation (DDA) [16–19], etc. have been successfully applied to the small-size fraction of the ice crystals. A survey of such works together with numerous references can be found, for example, in [20,21].

For the large-size fraction of the crystals, i.e. $s > 150$, the exact numerical methods become very computationally costly. In this case, the geometric-optics approximation becomes a reasonable approach and it is widely used for the optics of cirrus as well [21–24]. Obviously, the geometric-optics approximation does not resolve the fine angular structure of the scattered light caused by diffraction. This drawback of the geometric-optics approximation sometimes becomes an obstacle in the interpretation of experimental data. In particular, lidar signals mainly originate from the backscattering process. It was shown earlier [23,25] that the backscattering in the geometric optics approximation for the typical case of randomly oriented hexagonal ice columns and plates becomes an infinite quantity because of the corner-reflection effect. Therefore, to avoid this discrepancy, one should take into account the diffraction patterns that appear within the backward

* Corresponding author at: Tomsk State University, 36 Lenin Ave, 634050 Tomsk, Russia.
E-mail address: sasha_tvo@iao.ru (A. Konoshonkin).

http://dx.doi.org/10.1016/j.jqsrt.2016.12.024
0022-4073/

scattering direction.

To include diffraction to the problem of light scattering by large ice crystals of cirrus clouds $s > 150$, we extended the geometric-optics approximation to the physical-optics (PO) one [26–28] similarly as in the classical diffraction theory [29,30]. As a result, our PO code allowed us to resolve the above mentioned infinite backscattering of randomly oriented crystals [31]. It is worth noting that several other codes taking into account diffraction were developed in application to cirrus optics by other authors, too. In particular, the so-called improved geometric-optics method (IGOM) and the geometric-optics integral equation method (GOIE) have been used by Yang et al. [21] for long. However, it was recently noticed that the genuine IGOM code failed to calculate the backscattering for cirrus clouds [32], and the authors had to add an empirical correction [33]. Also, recently Bi et al. [34,35] have proposed the code which is similar to our PO code but it has not been applied yet to real cirrus clouds.

An advantage of the PO is its applicability to the particles with a large size parameter. Indeed, this approximation is based on the assumption that the scattered field on the particle surface is replaced by the field obtained by the geometric-optics laws. Of course, it is not valid for small particles $a \approx \lambda$ but with increasing size parameter, the scattered field both inside a crystal and on its surface approaches the geometric-optics value. The accuracy of this method increases with the magnitude of the size parameter. Thus, the PO seems to be the best method to calculate the optical properties of the large-size fraction of cirrus clouds, especially in terms of the calculation time.

In our previous paper [36] we have compared three formulations of the PO and proved that only the PO based on (E,M)-diffraction theory looks reliable. We also have briefly compared PO results for a particle with fixed orientation with results obtained by a numerically exact method – the discontinuous Galerkin time-domain (DGTD). That illustrative comparison showed that the agreement is quite good within three diffraction fringes but some discrepancies had to be studied thoroughly. The aim of this paper is to estimate accuracy and determinate the limits of applicability of the PO in the case of backscattering, which is crustal for lidar studies. We compare the PO solution with two solutions obtained independently by different exact numerical methods, namely, the DGTD (German coauthors) [37,38] and the FDTD (Japan coauthors) [10] to avoid a mistake. It is worth noting that there are other methods to compare with, e.g. T-matrix [13–15] or DDA [16–19], but we think that the comparison with these two independent methods is reliable. Since the capability of up-to-date computers allows one to solve effectively the light scattering problem by randomly oriented non-spherical particles using the exact numerical methods for size parameters up to $s \approx 150$, we compare light scattering by hexagonal ice plates of the diameters 10 μm ($s \approx 120$) and 5 μm ($s \approx 60$) at the incident wavelength of 0.532 μm. In this case, the accuracy of the PO is rather high and the solutions obtained by the exact numerical methods and the physical-optics one should be close. For simplicity, we did not take into account absorption.

The paper is organized as follows. Section 2 presents our PO code. Section 3 presents the comparison of the scattered fields obtained by the DGTD and FDTD methods and the PO for a particle with fixed orientation. In Section 4 the accuracy of the PO is numerically studied for the case of arbitrary oriented crystals. The question of appropriate averaging over particle orientations is also considered in the section. Conclusion summarizes the obtained results.

2. Physical-optics approximation

For convenience, this section gives a brief overview of our physical-optics approximation. The PO code is described in more details in the previous paper [36]. It is worth noting that we have changed the approximation as compared to [28,31,39] by replacing the E-diffraction theory for the (E,M)-diffraction theory. Moreover, this section gives more attention to the shadow-forming beam.

In the problem of light scattering by large particles, as compared with the incident wavelength, the PO can be strictly defined by means of two following steps [28]. First, the exact scattered field both inside the particle and on its surface should be replaced by the scattered field obtained within the geometric-optics approximation. Then, outside the particle, the scattered field is found as the result of the propagation of the field, which is determined on the particle surface, to any observation point using the Maxwell equations.

If a particle is faceted like an ice crystal of cirrus clouds, the geometric-optics field on the crystal surface consists of a set of plane-parallel beams with various polygonal shapes and localizations leaving the crystal facets in the different directions $\mathbf{n}_j$. In the far zone of the crystal, i.e. at the distance $R >> a^2/\lambda$, every beam undergoes the Fraunhofer diffraction according to the Maxwell equations. As a result, the diffraction pattern appears on the scattering direction sphere $\mathbf{n}$ around the initial propagation direction $\mathbf{n}_j$ for any beam.

Let the crystal be illuminated by the incident plane wave

$$\mathbf{E}_{inc}(\mathbf{r}) = \mathbf{E}_0 e^{ik\mathbf{n}_0\mathbf{r}}, \tag{1}$$

where $\mathbf{E}_{inc}(\mathbf{r})$ is the transverse electric field, $\mathbf{r}$ is a point in 3D space, and $k = 2\pi/\lambda$. In the far zone, the scattered field becomes the diverging spherical wave

$$\mathbf{E}_{scat}(\mathbf{r}) = \mathbf{F}(\mathbf{n})e^{ikR}/R, \tag{2}$$

where $R = |\mathbf{r}|$, $\mathbf{n} = \mathbf{r}/|\mathbf{r}|$ is the scattering direction, and $\mathbf{F}$ is the complex-valued scattering amplitude. The transformation of the incident wave of Eq. (1) into the scattered wave of Eq. (2) is generally described by the 2×2 complex-valued Jones matrix

$$\mathbf{F}(\mathbf{n}) = \mathbf{J}(\mathbf{n})\mathbf{E}_0. \tag{3}$$

Finding of the Jones matrix is the full solution to a scattering problem because the Jones matrix determines the scattered field for the arbitrary polarization of incident waves. It is often convenient to describe the polarization of an incident wave by the Stokes vector $\mathbf{I}$. In this case, the Stokes vector of the scattered wave is transformed by means of the 4×4 Mueller matrix $\mathbf{M}(\mathbf{n})$ like Eq. (3)

$$\mathbf{I}_{scat}(\mathbf{n}) = \mathbf{M}(\mathbf{n})\mathbf{I}_{inc}, \tag{4}$$

where the Mueller matrix can be expressed through the Jones matrix (see e.g., [40])

To determine the Jones or Mueller matrices explicitly, we need to consider the scattered field on the crystal surface in details. The geometric-optics scattered field on the crystal surface becomes obviously the superposition of the plane-parallel beams $\mathbf{E}^j(\mathbf{r})$, i.e.

$$\mathbf{E}_{scat}(\mathbf{r}) = \sum_0^\infty \mathbf{E}^j(\mathbf{r}). \tag{5}$$

Every beam, both on the crystal surface and in the near zone around the crystal, has the form of Eq. (1) except for its finite transverse size.

In the superposition of Eq. (5), the case of $j = 0$ is reserved for a specific component of the geometric-optics scattered field called the shadow-forming field [28].

Let us explain the useful concept of the shadow-forming field. This component appears automatically if one uses the general definition of the total field as the superposition of the incident and scattered waves:

$$\mathbf{E}(\mathbf{r}) = \mathbf{E}_{inc}(\mathbf{r}) + \mathbf{E}_{scat}(\mathbf{r}). \tag{6}$$

Indeed, for illustration, consider the non-illuminated (i.e. shaded) part of the crystal surface if the particle is absolutely absorbing. In this case, the total field obviously vanishes $\mathbf{E}(\mathbf{r}) = 0$ on the shaded part of the surface. Thus, we arrive at the following equation on the shaded part of the surface

$$\mathbf{E}_{scat}(\mathbf{r}) = -\mathbf{E}_{inc}(\mathbf{r}) \tag{7}$$

proving the appearance of the shadow-forming field.

Then consider a non-absorbing crystal. Here the scattered beams of the superposition (5) can leave the crystal surface from arbitrary facets and in arbitrary directions including the incident direction $\mathbf{n}_0$. We state that it is useful to complete the superposition of the geometric-optics scattered beams of Eq. (5) with the shadow-forming beam, which is strictly defined as

$$\mathbf{E}^0(\mathbf{r}) = \begin{cases} -\mathbf{E}_{inc}(\mathbf{r}) & \text{on the shaded part of the particle,} \\ 0 & \text{otherwise.} \end{cases} \tag{8}$$

Note that this concept is quite general; it is applicable to particles of arbitrary shapes and absorbing properties. In the near zone of a particle, the shadow-forming beam propagates in the same direction $\mathbf{n}_0$ as the incident wave of Eq. (1) but it is in the antiphase to the incident wave according to the factor of (-1). Its transverse shape exactly corresponds to the geometric-optics shade of the particle.

Thus, in other words, the shadow-forming component of Eq. (8) is the inevitable component of both geometric-optics and physical-optics approximations. In the light of this concept, a lot of optical phenomena become physically obvious. In particular, the phenomenon of the so-called anomalous diffraction [41] is readily explained by interference between the shadow-forming and transmitted beams [42], and so on.

Therefore, in the superposition of Eq. (5), the index $j = 0$ corresponds to the shadow-forming beam of Eq. (8), while the other beams $j > 0$ are found numerically, for example, using the beam-splitting code.

After the scattered field on a crystal surface is found, it is transformed to the far zone within the physical-optics approximation [36]. As known, if a scattered field is given on any particle surface S, this field in the arbitrary point $\mathbf{r}$ outside the particle is strictly determined as an integral over the surface, this integral being the consequence of the Maxwell equations (see, e.g.,[9], Eq. (10.87))

$$\mathbf{E}_{scat}(\mathbf{r}) = \int_S \left\{ \left(\mathbf{N}\cdot\nabla_{\mathbf{r}'} G(\mathbf{r},\mathbf{r}') - G(\mathbf{r},\mathbf{r}')\left(\mathbf{N}\cdot\nabla_{\mathbf{r}'}\right)\right\} \mathbf{E}_{scat}(\mathbf{r}')d\boldsymbol{\rho}', \tag{9}$$

where $\mathbf{N}(\mathbf{r}')$ is the outward normal to the surface, $G(\mathbf{r},\mathbf{r}')$ is the Green function of free space, and $d\boldsymbol{\rho}'$ is the area element of the surface S. In the far zone, where $|\mathbf{r}-\mathbf{r}'| \approx R - \mathbf{n}\mathbf{r}'$, Eq. (9) is reduced to the following integral for the scattering amplitude ([29], Eq. (10.92))

$$\mathbf{F}(\mathbf{n}) = [i/(2\lambda)]\mathbf{n} \times \int_S \exp(-ik\mathbf{n}\mathbf{r}')\{[\mathbf{N}\times\mathbf{E}_{scat}(\mathbf{r}')] + [(\mathbf{N}\times\nabla\times\mathbf{E}_{scat}(\mathbf{r}'))\times\mathbf{n}]/(ik)\}d\boldsymbol{\rho}'. \tag{10}$$

Substitution of the near-zone field of Eq. (5) in Eq. (10) transforms the scattered field into a superposition of diverging spherical waves with the scattering amplitudes

$$\mathbf{F}_j(\mathbf{n}) = \frac{i}{2\lambda} e^{i\xi_j}\mathbf{n}\times\left\{\left[\mathbf{N}_j\times\mathbf{E}_j\right] + \left[\mathbf{N}_j\times[(\mathbf{n}_j\times\mathbf{E}_j)\times\mathbf{n}]\right]\right\} \times \int_{S_j} \exp[ik(\mathbf{n}_j-\mathbf{n})\boldsymbol{\rho}_j]\eta_j(\boldsymbol{\rho}_j)d\boldsymbol{\rho}_j. \tag{11}$$

where η is the shape function.

It is worth noting that in the classical theory of diffraction dealing with the transmission of any incident wave through a hole in a screen, the integral (10) with the substitution of $\mathbf{E}_{scat}(\mathbf{r}') \approx \mathbf{E}_{inc}(\mathbf{r}')$ is called the Kirchhoff approximation, the (E,M)-diffraction theory. Here two other approximations associated with names of Rayleigh and Sommerfeld (the E and M diffraction theories) are often used when only one of the terms enclosed in the square brackets in Eq. (11) remains after doubling [29,30].

In our previous papers [31,39], within the E-diffraction theory, we used only the first doubled term of Eq. (11) since both terms of Eq. (11) were approximately equal for the small scattering angles $\mathbf{n} \approx \mathbf{n}_j$. However, when a beam leaves a crystal facet at the grazing angle, both terms become noticeably different. Therefore, in the light scattering problem, Eq. (11) including both the terms seems to be more reasonable, see [36]. Indeed, an argument in favor of both terms is that they both follow directly from the Maxwell equations.

Thus, our PO algorithm calculating the field scattered by an ice crystal consists of two parts. First, all characteristics of the plane-parallel beams leaving a crystal surface are found by means of the beam-splitting code [43]. Second, the diffraction of the beams is calculated using Eq. (11).

3. Normally illuminated hexagonal ice plate

For comparison of solutions to the light scattering problem by different numerical methods, we consider the simplest case of normal illumination of a hexagonal ice plate (Fig. 1). The incident wavelength is 0.532 μm and the refractive index is assumed as 1.3116. Two diameters of the plate of 10 μm and 5 μm with the plate thicknesses of 5.79 μm and 2.895 μm, respectively, are used.

As shown in Fig. 1(a), here only three plane-parallel beams are formed in the near zone of the crystal. They are the shadow-forming $\mathbf{E}^{(0)}$, the forward scattered $\mathbf{E}^{(1)}$ and the backscattered $\mathbf{E}^{(2)}$ beams

$$\mathbf{E}^{(0)}(x) + \mathbf{E}^{(1)}(x) = (-1 + te^{i\xi_1})\eta(y,z)e^{ikx}\mathbf{E}_0 \quad \text{at } x > l/2, \tag{12}$$

$$\mathbf{E}^{(2)}(x) = re^{i\xi_2}\eta(y,z)e^{-ikx}\mathbf{E}_0 \quad \text{at } x < -l/2, \tag{13}$$

where l is the crystal thickness and t and r are the transmissivity and reflectivity, respectively, obeying the energy conservation law $t^2 + r^2 = 1$ for non-absorptive crystals.

Amplitudes and phases of the forward and backward scattered beams can be taken from the well-known problem of transmission and reflection of light for a plane-parallel plate. Otherwise, this reflected and transmitted light can be obtained as a series of successive acts of re-reflections inside the crystal by the front and rear facets that is easily modeled by the beam-splitting code. In our calculations, we limit the beam-splitting code by 10 reflected/refracted events which correspond to more than 99.99% scattered energy. In the far zone, the surface integral of Eq. (11) corresponds to the diffraction pattern from a hexagonal hole in a screen shown in Fig. 1(b).

The scattered field at any direction $\mathbf{n}$ is characterized, in general, by the 2×2 complex-valued Jones matrix of Eq. (3) or by the real-valued 4×4 Mueller matrix of Eq. (4). The intensities of the scattered field in any scattering direction obtained by the PO and the DGTD method are presented in Fig. 2. We see that the scattered fields match each other qualitative, however, there is some quantitative difference.

To avoid comparison of these 2D numerical data, we have averaged the Mueller matrices over the azimuth angle φ. The above Mueller matrices also correspond to averaging over crystal

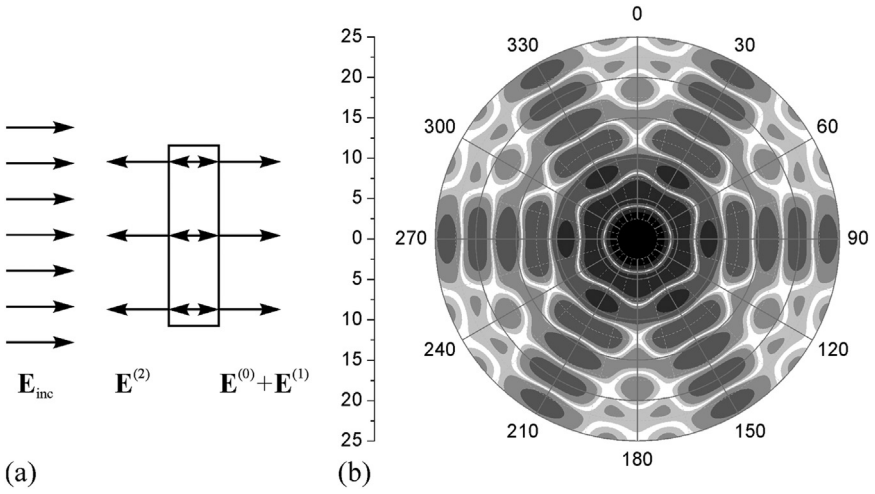

Fig. 1. Scattering by a hexagonal plate in the PO: (a) plane-parallel beams in the near zone; (b) the Fraunhofer diffraction pattern in the wave zone (the plate diameter is 10 μm, the wavelength is 0.532 μm, and the scale indicates the scattering angles relative to the forward direction).

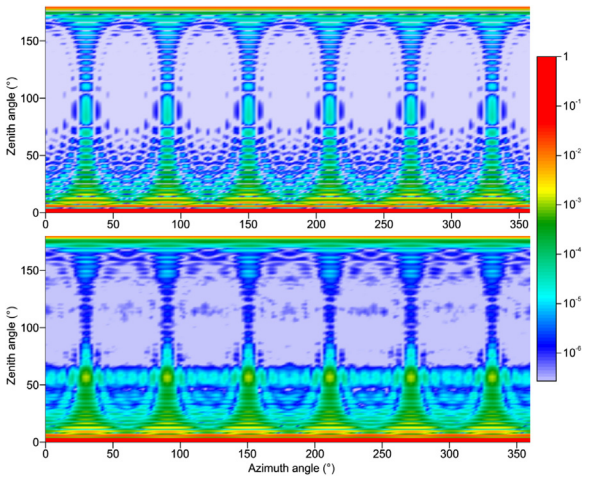

Fig. 2. The intensity of the scattered light on the scattering direction sphere obtained by the PO (upper) and by the DGTD method (lower).

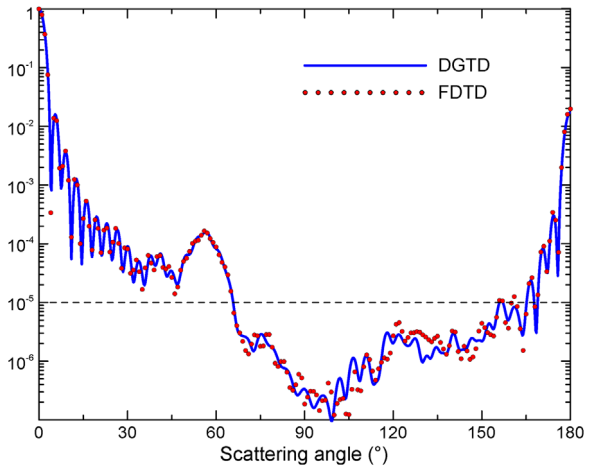

Fig. 3. The normalized differential scattering cross section obtained by the DGTD and FDTD methods for the plate of the diameter $D = 10$ μm.

rotation around the x- axis. As known [40–42], the averaged matrices for particles having plane of symmetry have 6 independent non-zero elements

$$\mathbf{M}(\theta) = \begin{pmatrix} M_{11}(\theta) & M_{12}(\theta) & 0 & 0 \\ M_{12}(\theta) & M_{22}(\theta) & 0 & 0 \\ 0 & 0 & M_{33}(\theta) & M_{34}(\theta) \\ 0 & 0 & -M_{34}(\theta) & M_{44}(\theta) \end{pmatrix}, \tag{14}$$

where $M_{11}(\theta)$ is the differential scattering cross-section and the other elements are responsible for polarization.

The normalized differential scattering cross section $M'_{11}(\theta) = M_{11}(\theta)/M_{11}(0)$ obtained by two exact methods for the plate diameter of 10 μm is presented in Fig. 3. It should be noted that the results of the comparison of the DGTD and the PO for the 10 μm particle have already been presented in [36]. Here we compare these results with the FDTD and pay more attention to the forward and backward scattering directions. We see that these data completely coincide with each other for the quantities larger than 10^{-5}. On the one hand, this fact proves reliability of both methods. On the other hand, it shows accuracy of the data obtained. Namely, the small values of $M'_{11}(\theta)$ that are less than 10^{-5} within the interval 70–175° of the scattering angles reveal some dispersion. Consequently, the quantity 10^{-5} can be assumed as the low limit of these calculations. The discrepancy of these two numerically exact methods within the interval 70–175° of the scattering angles is caused by differences of particle discretization or imperfection of numerical integration procedures of these methods. Moreover, these two methods are numerical and the difference is close to numerical accuracy. One can see that the results of the DGTD and the FDTD seems to be different for the first diffraction minimum at the point of about 4 degrees (Fig. 3), but Fig. 5 shows that this discrepancy is due to small spatial resolution of the solutions.

Fig. 4 shows the comparison of the same values as in Fig. 3 obtained by the DGTD and the PO methods. In this case, the data agree with each other for the quantities larger than 10^{-4}. This agreement takes place near the forward and backward scattering directions that are the propagation directions of the near-zone beams (Fig. 1(a)).

For a detailed study of this agreement, the vicinities of the forward and backward scattering directions are shown in Figs. 5 and 6 at an expanded scale. To interpret these data, let us come back to Fig. 1(b) where the scattering or diffraction pattern is shown without averaging over the azimuth angle φ. As known [29,30], any Fraunhofer diffraction pattern consists of diffraction fringes of different orders. Numbering the fringes from the center, let us attribute the first order to the central bright fringe of Fig. 1 (b), the second order to the next bright fringe, and so on. Comparing Figs. 1(b) and 4 we see that the bright fringes in Fig. 4 are

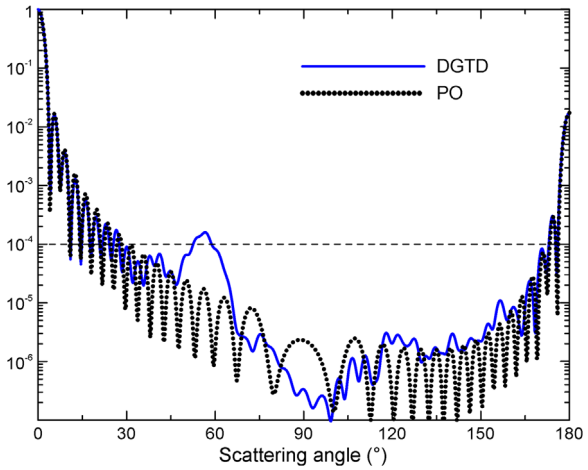

Fig. 4. The differential scattering cross section obtained by the DGTD method and the PO for the plate of the diameter $D=10$ μm.

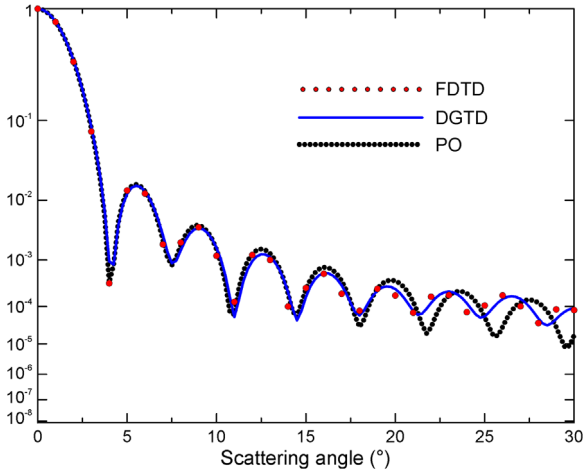

Fig. 5. The differential scattering cross section in the vicinity of the forward directions for the plate of the diameter $D=10$ μm.

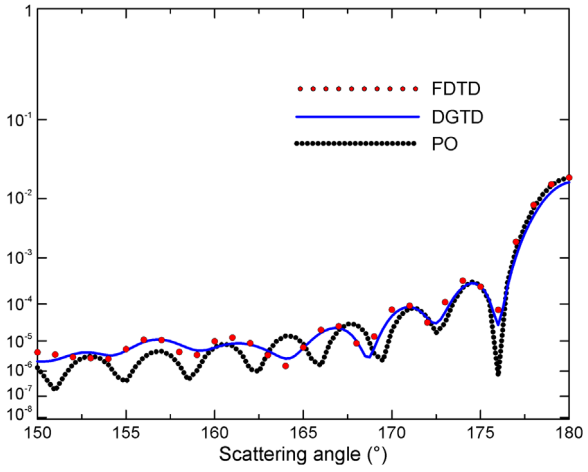

Fig. 6. The same differential scattering cross section as in Fig. 5 in the vicinity of the backward direction.

formed just by the bright fringes of Fig. 1(b) of the same order.

Thus, Fig. 5 proves that the PO and the exact methods agree very closely within 5 diffraction fringes near the forward direction. As for the backward direction shown in Fig. 6, the data coincide within 3 diffraction fringes.

This coincidence can be easily explained [36]. Indeed, the PO assumes that the scattered field in the near zone is the step-like function due to the shape function of Eq. (11). The same shape function is used in the classical theory of diffraction dealing with penetration of light through a hole in a screen [29,30]. As known in the diffraction theory, the main difference between the incident and the exact fields inside the hole is that the step of the incident field at the edge of the hole should be replaced by a narrow strip of thickness of a few wavelengths smoothing this step. In the far zone, this strip does not practically correct the diffraction fringes of the low orders shifting the corrections to the fringes of the higher orders. Since the strip thickness weakly depends on the hole diameter, the border of corrections depends, mainly, on the size parameter. In particular, when the size parameter is larger, the border of corrections is shifted to higher fringe orders.

It is obvious that in the light scattering problem, the strip also should appear in the exact field formed on an exit crystal facet. As a result, the diffraction fringes of low orders obtained by the PO agree well with the data obtained by the exact methods. The border of corrections of the diffraction fringes depends on the crystal size parameters. This statement is supported by the comparison of the data in Figs. 4 and 7 obtained for the crystals of the diameters of 10 μm and 5 μm with size parameters $s=120$ and $s=60$, respectively. We see in Fig. 7 that in the case of the diameter of 5 μm that the corrections become essential in the third fringe near the forward direction and in the second fringe near the backward one.

In addition to the distortions of the Fraunhofer diffraction fringes near the forward and backward directions, the exact solutions in Figs. 4 and 7 also demonstrate two hills at large scattering angles of about 60 and 120°. These hills cannot be explained by the strips. They should be associated with some transverse structure of the exact scattered field on the exit facets which is unknown. However, these hills are obtained for the fixed crystal orientation, which is hardly interesting for practice. Moreover, their magnitudes decrease with the crystal size parameter as shown in Figs. 4 and 7. Therefore, the main result of this section is that the PO and the exact methods coincide in the vicinity of the scattering directions corresponding to the geometric-optics propagation directions of the plane-parallel beams of the near zone. The minimal limit of applicability of PO is about $s\approx 100$.

In addition to the normalized scattering cross sections shown in the above figures, all elements of the Mueller matrices were calculated using both the exact and the PO methods as well. These elements reveal similar regularities. As an example, Figs. 8 and 9 present the normalized quantity $M'_{33}(\theta)=M_{33}(\theta)/M_{11}(0)$ in the

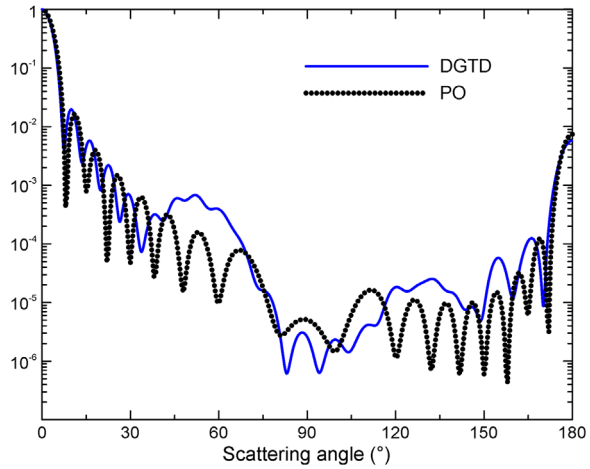

Fig. 7. The same data as in Fig. 4 for the plate of the diameter $D=5$ μm.

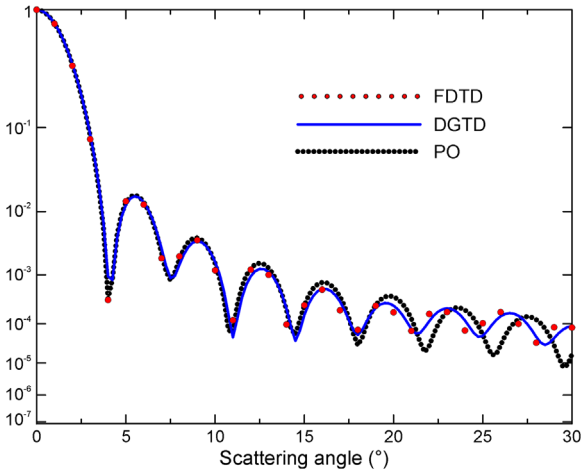

Fig. 8. The same data as in Fig. 5 for the normalized element M_{33}.

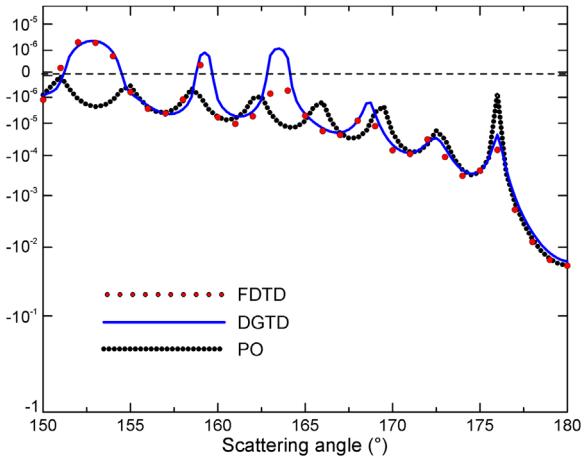

Fig. 9. The same data as in Fig. 6 for the normalized element M_{33}.

vicinity of the forward and backward scattering directions. As in Figs. 5 and 6, we obtain close agreement between the PO and the numerically exact quantities within 5 diffraction fringes in the forward direction and 3 diffraction fringes in the backward one. In Fig. 9, the value $M_{33}(\theta)$ is negative in the PO while the exact methods at $\theta < 165^\circ$ give small positive quantities of about 10^{-6}. This discrepancy could be caused by either inaccuracy of the PO or by round-off errors of the exact methods for the small quantities. The other diagonal elements of the Mueller matrix show the same regularities as in Figs. 8 and 9. As for the off-diagonal elements, they are small (10^{-4}) and dispersed. Therefore, they are not presented.

Thus, we have shown that the accuracy of the PO depends on the size parameter of a crystal particle, with the accuracy increasing with the size parameter. In particular, for the hexagonal ice plate of the diameter of 10 μm and the wavelength of 0.532 μm, the PO gives reliable data within, at least, 3 diffraction fringes.

4. Averaging over crystal orientations

In Section 3, we have considered the case of a crystal with a fixed spatial orientation. This case is of no practical interest since orientations of the ice crystals occurring in the atmosphere are always statistically distributed according to some laws. These laws are changed from the preferably horizontal orientation, on the one side, to the random orientation, on the other side.

The drawback of any exact numerical method solving the problem of light scattering by the ice crystals is its computational cost for a given crystal orientation. Therefore, averaging of the Mueller matrix over crystal orientations using the exact methods becomes a challenging problem. On the contrary, it can be solved at moderate computational costs by the PO.

To begin with, let us answer the question: how many orientations are needed to make an appropriate averaging? The geometric optics solutions for randomly oriented particles usually average over thousands or billions orientations [43], i.e. Macke used 30000 orientations [22]. Some exact numerical solutions take into account few orientations, i.e. Liu takes 48 orientations [44], Collier takes 6 orientations [45].

Averaging over particle orientations means averaging over three Euler angles: α, β, γ[46]. For the exact backscattering direction, which is important for lidar studies, averaging over α angle can be done analytically. Moreover, it has no effect on the differential scattering cross section. Taking into account the symmetry of a hexagonal particle, the number of orientations for the γ angle decreases 6 times, and for the β angle it is twice as little.

Now let us have a look at the typical dependence of the differential scattering cross section in the backscattering direction on the slope angle β after averaging over γ angle (Fig. 10). Here we can see three different parts: the first one (0–10°) is the oscillations caused by the diffraction on the hexagonal facet of the crystal; the second one (10–87°) is the corner reflection predomination [46,47]; the third one (87–90°) is the oscillations caused by the diffraction on the rectangular facets of the crystal. We can see that appropriate averaging requires, at least, 3 points on each diffraction fringe.

Now let us show the dependence of the averaged differential scattering cross section in the exact backscattering direction on the number of particle orientations, see Fig. 11. Here, for simplicity, we let the same number of orientations for both β and γ angle intervals. One can suppose that the solution converges at 576 (24x24) orientations. To refute this assumption, Fig. 12 shows the profile for 4624 (68x68) orientations (blue line). We can see in Fig. 11 that only two points fall on the first diffraction fringe and the differential scattering cross section cannot be integrated properly. Appropriate averaging for the 10 μm particle, in this case, has to be done over more than 17161 (131x131) orientations. Our calculations show that the same is true for all the Mueller matrix elements. In spite of the fact that the above mentioned results were obtained within the PO, any exact numerical solution requires no fewer orientations for spatial averaging.

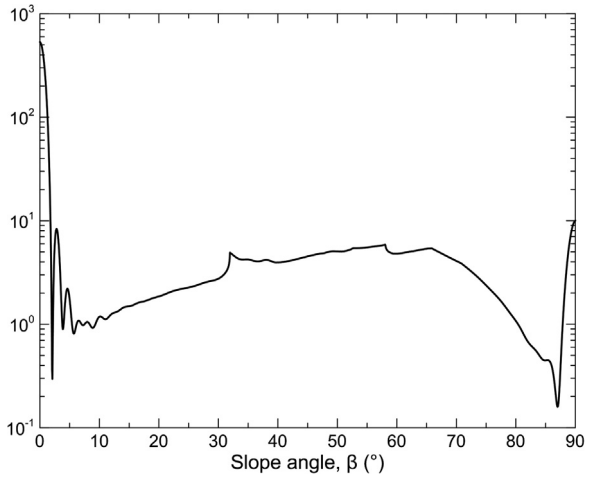

Fig. 10. The typical dependence of the differential scattering cross section in the backscattering direction after averaging over γ angle for 10 μm particle.

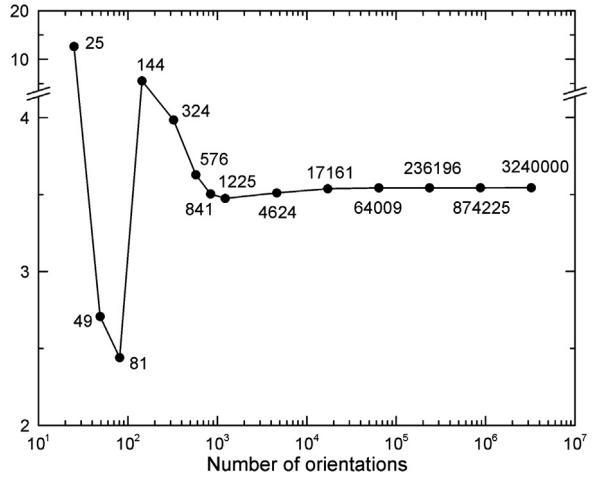

Fig. 11. The averaged differential scattering cross section in the exact backscattering direction depending on the number of particle orientations.

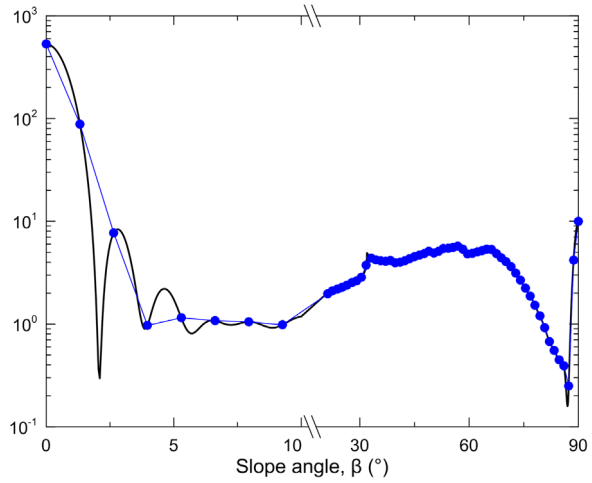

Fig. 12. The approximation of the real (black) differential scattering cross section by 4624 orientations (blue).

Our calculations show that for a hexagonal ice plate, the angular size of the first diffraction fringe ξ depends on the particle diameter (D) through the simple relation

$$\xi = 0.69\frac{\lambda}{D}\cdot\frac{180^\circ}{\pi} \tag{15}$$

which is in good agreement with the classical solution of the angular size of diffraction on a circular aperture [48].

Therefore, taking into account the symmetry of a hexagonal particle one can easily estimate the number of the orientations needed for appropriate averaging in the case of a uniform angular step:

$$N_{orient} \approx \frac{90^\circ}{0.3\xi}\cdot\frac{60^\circ}{0.3\xi} \tag{16}$$

which makes 13,600 orientations for a 10 μm particle and 1,360,000 orientations for a 100 μm particle at the wavelength of 0.532 μm. Since the exact numerical solution of light scattering for one particle orientation is a problem of hours [49,50], averaging over 13,600 orientations for a randomly oriented particle is a problem of years. At the same time, we have averaged more than 10^6 orientations within the PO for less than 3 hours on a desktop Core i3-3.7Ghz.

Since there is no available matrix that has been calculated by the exact methods for randomly oriented particle with appropriate averaging, we cannot compare the numerical data for the randomly oriented particle as it was done in Section 2. Nevertheless, some estimation can be obtained within the framework of the PO.

In Section 2 we show that the PO gives reliable results only within a finite domain of the scattering directions. Therefore, one might suppose that the accuracy of the PO for the averaged Mueller matrices is low. In reality, the situation is the opposite. Indeed, consider, for example, the case of random crystal orientations. Here any scattered field of Eq. (11) moves on the scattering direction sphere more or less uniformly because of the random orientations. As a result, an observer detects some integrated value rather than the values for a fixed crystal orientation.

In this section, we show that the accuracy of the PO is rather high for the averaged backscattering Mueller matrices because of the integration of the diffraction patterns.

Let us consider the following scheme often used in practice. A vertically pointing lidar sounds the hexagonal ice plates whose orientations can be continuously varied from the horizontal to random ones [51,52]. The probability distribution function over orientations is assumed as follows. Denote the plate tilt as $\beta = \arccos(\mathbf{z}\cdot\mathbf{N})$, where $\mathbf{z}$ is the vertical directed upward and $\mathbf{N}$ is the normal to a hexagonal facet. Assume that the plate orientations are uniformly distributed relative to the rotations about both the normal $\mathbf{N}$ and the vertical $\mathbf{z}$, γ and α angles respectively. As for the particle tilts, we assume the truncated Gaussian probability distribution with the effective tilt angle β_{eff}

$$p(\alpha,\beta,\gamma) = \frac{1}{2\pi}\cdot\frac{1}{2\pi} \cdot\exp(-\beta^2/2\beta_{eff}^2)/\int_0^{\pi/2}\exp(-\beta^2/2\beta_{eff}^2)\sin\beta d\beta, \tag{17}$$

where the limit cases $\beta_{eff} = 0$ and $\beta_{eff} = \pi/2$ correspond to either horizontal or quasi-random orientations, respectively.

Lidars detect only the backscattering described by the Mueller matrix $\mathbf{M}(\pi)$. As known [40,41], for the given orientation distribution, the symmetry reduces the averaged Mueller matrix for vertically pointed lidars to the diagonal view

$$\mathbf{M}(\pi) = \sigma\begin{pmatrix} 1 & 0 & 0 & 0 \\ 0 & 1-d & 0 & 0 \\ 0 & 0 & d-1 & 0 \\ 0 & 0 & 0 & 2d-1 \end{pmatrix}. \tag{18}$$

Here only two quantities, the backscattering cross section σ and the depolarization parameter d, can be obtained from measurements. The linear δ_l and circular δ_c depolarization ratios are simply connected with the depolarization parameter:

$$\delta_l = d/(2-d),$$
$$\delta_c = d/(1-d). \tag{19}$$

In our PO code, we first calculate 16 elements of the backscattering Mueller matrix for all crystal orientations. Then these matrices are averaged numerically according to the given orientation probability distribution of Eq. (17). Finally, we obtain the quantities σ and d of Eq. (18) that are detected in lidar research.

Our estimation of the accuracy of the PO is based on the following physical arguments. When one considers any integral of the Fraunhofer diffraction pattern like Fig. 1(b), this integral is formed predominantly by the contributions from a few fringes of a low order. The diffraction fringes of high orders give usually negligible contribution. In the case of a circle, for example, three first fringes give 84%, 7%, and 3% of the exact magnitude of the integral, respectively, while about 5% are contributed by the other fringes.

We have calculated the quantities σ and d using our PO code with three different scattering amplitudes of Eq. (11): $\mathbf{F}$, $\mathbf{F}_3$ and $\mathbf{F}_5$

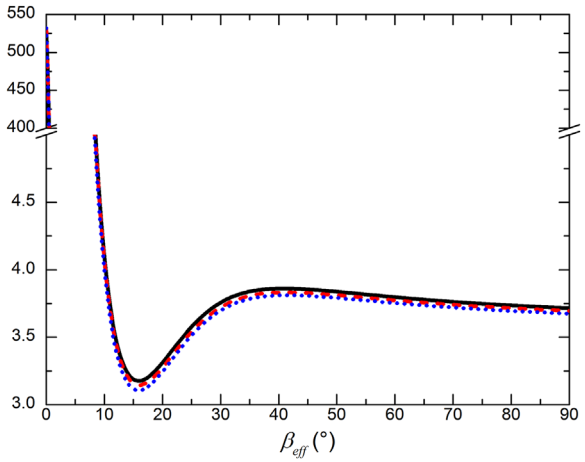

Fig. 13. The backscattering cross section (μm^2/ster) for the arbitrary oriented hexagonal ice plate of the diameter $D = 10$ μm; **F** (solid), $\mathbf{F}_5$(dashed) and $\mathbf{F}_3$(dotted) depending on the effective tilt angle β_{eff}.

where **F** is the exact function while $\mathbf{F}_3$ and $\mathbf{F}_5$ are the functions truncated by the diffraction fringes of more than the 3-d and 5-th orders, respectively. The order of the fringes is easily found using our code as an integer part of the ratio $(\mathbf{n}_j - \mathbf{n})\boldsymbol{\rho}_j/\lambda$ in the integrand of Eq. (11). Here, for example, the function $\mathbf{F}_5$ includes the diffraction fringes up to the 5-th order and discards the fringes of higher orders.

The results are presented in Figs. 13–16. We see that the contribution of the fringes of more than the 3-d order is less than about 2% of the quantities calculated with the exact function **F**. Consequently, the quantities σ and d obtained are the results of integration mainly of the diffraction fringes of no more than the 3-d order. As known for the circular beams, the integral of three diffraction fringes approach the total integral with the accuracy of 95%. Though the near-zone beams for the crystals are not circular, averaging over orientations should smooth the dependence on the beam shapes. Consequently, similarly, we can suppose that the accuracy of the data shown in Figs. 13–16 should be no worse than 95% of the data that could be obtained by the exact methods. This conclusion is valid for the crystals with the size parameter more than 20 according to the discussion in Section 2.

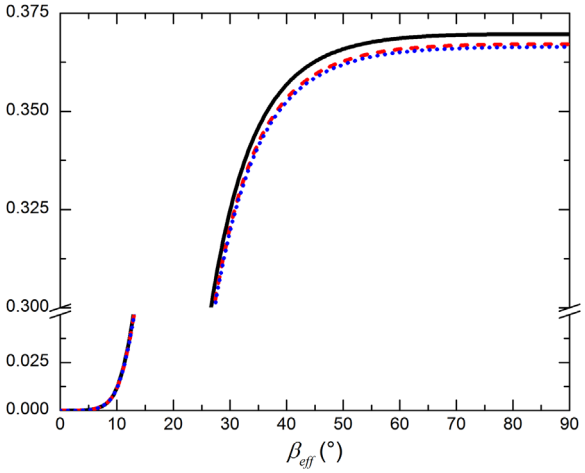

Fig. 14. The depolarization parameter for the arbitrary oriented hexagonal ice plate of the diameter $D = 10$ μm depending on the effective tilt angle β_{eff}.

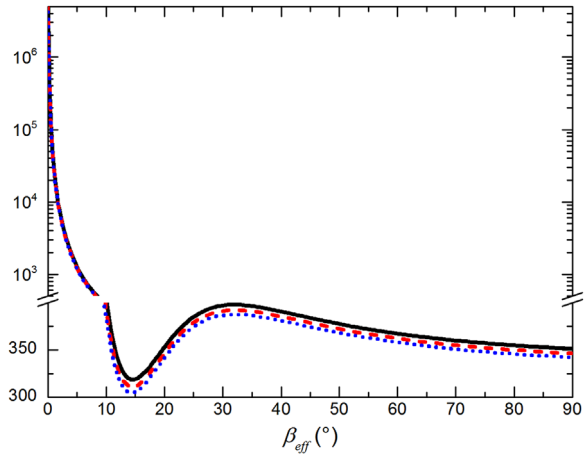

Fig. 15. The same data as in Fig. 13 for $D = 100$ μm.

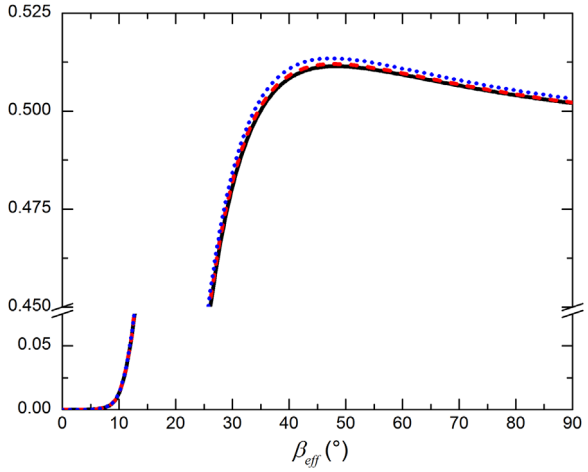

Fig. 16. The same data as in Fig. 14 for $D = 100$ μm.

5. Conclusion

The exact numerical methods solving the problem of light scattering by ice crystals of cirrus clouds using the Maxwell equations are effective only if the size parameter is less than 150. The physical-optics approximation, on the contrary, is effective for large values of the size parameter. In this paper we have succeeded in comparing these methods for the size parameters of about 120, where both approaches overlap.

We show, that the exact and physical-optics solutions agree very closely within several first diffraction fringes about the centers of the diffraction patterns. In particular, for the size parameter of 120 the diffraction fringes of the physical-optics approximation deviate from the exact counterparts beginning from the fourth diffraction fringe. As a result, the accuracy of the physical-optics approximation for the backscattering Mueller matrix averaged over crystal orientation is estimated as 95% for the crystals with the size parameter larger than 120. We also showed that the PO should not be applied to the particle with the size parameter less than 100 because of the accuracy issue.

We have derived a simple expression that allows one to estimate the minimal number of particle orientations required for appropriate spatial averaging. We have also showed that for a typical particle of cirrus cloud, which is a 100 μm (the size parameter is about 1200) randomly oriented hexagonal ice crystal, over a billion orientations are needed for appropriate averaging in the case of uniform spatial grid. This makes the exact numerical

methods inapplicable to solve the problem of visible light scattering by crystals of cirrus clouds because of their computational cost. In this situation, the physical optics approximation looks a very promising tool.

Funding information

Russian Foundation for Basic Research (15-05-06100, 15-55-53081, 16-35-60089); Russian Science Foundation (14-27-00022) in the development of the computer code used for calculations in Section 4; Collaboration Research Program of the Research Institute for Applied Mechanics, Kyushu University (no. 10, 2014; no. 8, 2015); JSPS Kakenhi Grant (25247078).

Acknowledgment

The authors gratefully acknowledge the computing time granted by the Paderborn Center for Parallel Computing (PC2).

References

[1] Liou KN. Influence of cirrus clouds on weather and climate processes: a global perspective. Mon Weather Rev 1986;114:1167–1199.
[2] Stephens GL, Tsay SC, Stackhouse PW, Flatau PJ. The relevance of the microphysical and radiative properties of cirrus clouds to climate and climatic feedback. J Atmos Sci 1990;47:1742–1754.
[3] Liou KN. An introduction to atmospheric radiation. London: Academic Press; 2002.
[4] Zhou C, Dessler AE, Zelinka MD, Yang P, Wang T. Cirrus feedback on interannual climate fluctuations. Geophys Res Lett 2014;41:9166–9173.
[5] Ding J, Yang P, Holz RE, Platnick S, Meyer KG, Vaughan MA, Hu Y, King MD. Ice cloud backscatter study and comparison with CALIPSO and MODIS satellite data. Opt Express 2016;24:620–636.
[6] Auer AH, Veal DL. The dimension of ice crystals in natural clouds. J Atmos Sci 1970;27:919–926.
[7] Mitchell DL. Use of mass- and area-dimensional power laws for determining precipitation particle terminal velocities. J Atmos Sci 1996;53:1710–1723.
[8] Yee SK. Numerical solution of initial boundary value problems involving Maxwell's equations in isotropic media. IEEE Trans Antennas Propag 1966;14:302–307.
[9] Ishimoto H, Zaizen Y, Uchiyama A, Masuda K, Mano Y. Shape modeling of mineral dust particles for light scattering calculations using the spatial Poisson–Voronoi tessellation. J Quant Spectrosc Radiat Transf 2010;111:2434–2443.
[10] Ishimoto H, Masuda K, Mano Y, Orikasa N, Uchiyama A. Irregularly shaped ice aggregates in optical modeling of convectively generated ice clouds. J Quant Spectrosc Radiat Transf 2012;113:632–643.
[11] Taflove A, Hagness SC. Computational Electrodynamics: The Finite-Difference Time-Domain Method. 2nd ed.. Norwood: Artech House; 2000.
[12] Sun W, Fu Q, Chen Z. Finite-difference time-domain solution of light scattering by dielectric particles with a perfectly matched layer absorbing boundary condition. Appl Opt 1999;38:3141–3151.
[13] Waterman PC. Matrix formulation of electromagnetic scattering. Proc IEEE 1965;53:805–812.
[14] Mishchenko MI, Travis LD, Mackowski DW. T-matrix computations of light scattering by nonspherical particles: a review. J Quant Spectrosc Radiat Transf 1996;55:535–575.
[15] Havemann S, Baran AJ. Extension of T-matrix to scaterring of electromagnetic plane waves by non-axisymmetric dielectric particles: application to hexagonal ice cylinders. J Quant Spectrosc Radiat Transf 2001;70:139–158.
[16] Purcell EM, Pennypacker CR. Scattering and absorption of light by nonspherical dielectric grains. Astrophys J 1973;186:705–714.
[17] Yurkin MA, Hoekstra AG. The discrete dipole approximation: an overview and recent developments. J Quant Spectrosc Radiat Transf 2007;106:558–589.
[18] Okamoto H. Information content of the 95-GHz cloud radar signals: theoretical assessment of nonsphericity and error evaluation of the discrete dipole approximation. J Geophys Res 2002;107 [AAC 4-1–AAC 4-16].
[19] Sato K, Okamoto H. Characterization of Ze and LDR of non-spherical and inhomogeneous ice particles for 95-GHz cloud radar: its application to microphysical retrievals. J Geophys Res 2006;111:D22213.
[20] Mishchenko MI, Hovenier JW, Travis LD. Light scattering by nonspherical particles: theory, measurements, and applications.San Diego: Academic Press; 2000.
[21] Yang P, Bi L, Baum BA, Liou K-N, Kattawar GW, Mishchenko MI, Cole B. Spectrally consistent scattering, absorption, and polarization properties of atmospheric ice crystals at wavelengths from 0.2 to 100 μm. J Atmos Sci 2013;70:330–347.
[22] Macke A, Mueller J, Raschke E. Single scattering properties of atmospheric ice crystal. J Atmos Sci 1996;53:2813–2825.
[23] Takano Y, Liou KN. Solar radiative transfer in cirrus clouds. Part I: single-scattering and optical properties of hexagonal ice crystals. J Atmos Sci 1989;46:3–19.
[24] Muinonen K, Nousiainen T, Fast P, Lumme K, Peltoniemi JI. Light scattering by Gaussian random particles: ray optics approximation. J Quant Spectrosc Radiat Trans 1996;55:577–601.
[25] Borovoi G, Kustova NV, Oppel UG. Light backscattering by hexagonal ice crystal particles in the geometrical optics approximation. Opt Eng 2005;44:071208.
[26] Iwasaki S, Okamoto H. Analysis of the enhancement of the backscattering by nonspherical particles with flat surfaces. Appl Opt 2001;40:6121–6129.
[27] Borovoi G, Grishin IA. Scattering matrices for large ice crystal particles. J Opt Soc Am A 2003;20:2071–2080.
[28] Borovoi A, Konoshonkin A, Kustova N. The physical-optics approximation and its application to light backscattering by hexagonal ice crystals. J Quant Spectrosc Radiat Transf 2014;146:181–189.
[29] Jackson JD. Classical Electrodynamics. 3rd ed.. Berkeley: Wiley & Sons; 1999.
[30] Nieto-Vesperinas M. Scattering and diffraction in physical optics.New Jersey: World sci; 2006.
[31] Borovoi A, Konoshonkin A, Kustova N. Backscattering by hexagonal ice crystals of cirrus clouds. Opt Lett 2013;38:2881–2884.
[32] Ding J, Yang P, Holz RE, Platnick S, Meyer KG, Vaughan MA, Hu Y, King MD. Ice cloud backscatter study and comparison with CALIPSO and MODIS satellite data. Opt Express 2016;24:620–636.
[33] Zhou C, Yang P. Backscattering peak of ice cloud particles. Opt Express 2015;23:11995–12003.
[34] Bi L, Yang P, Kattawar GW, Hu Y, Baum BA. Diffraction and external reflection by dielectric faceted particles. J Quant Spectrosc Radiat Transf 2011;112:163–173.
[35] Bi L, Yang P, Kattawar GW, Hu Y, Baum BA. Scattering and absorption of light by ice particles: solution by a new physical-geometric optics hybrid method. J Quant Spectrosc Radiat Transf 2011;112:1492–1508.
[36] Konoshonkin AV, Kustova NV, Borovoi AG, Grynko Y, Förstner J. Light scattering by ice crystals of cirrus clouds: comparison of the physical optics methods. J Quant Spectrosc Radiat Transf 2016;182:12–23.
[37] Hesthaven JS, Warburton T. Nodal High-Order Methods on Unstructured Grids: I. Time-Domain Solution of Maxwell's Equations. J Comp Phys 2002;181:186–221.
[38] Grynko Y, Shkuratov Y, Förstner J. Light scattering by randomly irregular dielectric particles larger than the wavelength. Opt Lett 2013;38:5153–5156.
[39] Borovoi A, Konoshonkin A, Kustova N. Backscattering reciprocity for large particles. Opt Let 2013;38:1485–1487.
[40] Mishchenko MI, Travis LD, Lacis AA. Scattering, absorption, and emission of light by small particles.Cambridge: Cambridge university press; 2002.
[41] van de Hulst H. Light scattering by small particles.New York: Wiley; 1981.
[42] Borovoi AG. Light scattering by large particles: physical optics and the shadow-forming field. In: Kokhanovsky AA, editor. Light Scattering Reviews, 8. Chichester: Springer-Praxis; 2013. p. 115–138.
[43] Konoshonkin AV, Kustova NV, Borovoi AG. Beam-splitting code for light scattering by ice crystal particles within geometric-optics approximation. J Quant Spectrosc Radiat Transf 2015;164:175–183.
[44] Liu C, Panetta RL, Yang P. Application of the pseudo-spectral time domain method to compute particle single-scattering properties for size parameters up to 200. J Quant Spectrosc Radiat Transf 2012;113:1728–1740.
[45] Collier CT, Hesse E, Taylor L, Ulanowski Z, Penttilä A, Nousiainen T. Effects of surface roughness with two scales on light scattering by hexagonal ice crystals large compared to the wavelength: DDA results. J Quant Spectrosc Radiat Transf 2016;182:225–239.
[46] Borovoi A, Konoshonkin A, Kustova N. Backscatter ratios for arbitrary oriented hexagonal ice crystals of cirrus clouds. Opt Lett 2014;39:5788–5791.
[47] Borovoi A, Kustova N, Konoshonkin A. Interference phenomena at backscattering by ice crystals of cirrus clouds. Opt Express 2015;23:24557–24571.
[48] Born M, Wolf E. Principles of Optics. 4th ed.. London: Pergamon Press; 1970.
[49] Yurkin MA, Maltsev VP, Hoekstra AG. The discrete dipole approximation for simulation of light scattering by particles much larger than the wavelength. J Quant Spectrosc Radiat Transf 2007;106:546–557.
[50] Yurkin MA, Hoekstra AG. The discrete-dipole-approximation code ADDA: capabilities and known limitations. J Quant Spectrosc Radiat Transf 2011;112:2234–2247.
[51] Hunt WH, Winker DM, Vaughan MA, Powell KA, Lucker PL, Weimer C. CALIPSO lidar description and performance assessment. J Atmos Ocean Technol 2009;26:1214–1228.
[52] Noel V, Chepfer H, Ledanois G, Delaval A, Flamant PH. Classification of particle effective shape ratios in cirrus clouds based on the lidar depolarization ratio. Appl Opt 2002;41:4245–4257.